RSC Advances

PAPER

View Article Online
View Journal | View Issue

Cite this: *RSC Adv.*, 2023, **13**, 10135

An accuracy improved ratiometric SERS sensor for rhodamine 6G in chili powder using a metal–organic framework support†

Yangjie Chen,[ab] Juan Hao,[ab] Zhihang Yin,[ab] Qinghui Wang,[bc] Youting Zhou,[ab] Lingpu Jia,[bd] Huiming Li,[bc] Wenlong Liao*[bc] and Kunping Liu *[ab]

Internal standard molecule 4-mercaptobenzoic acid (4-MBA) embedded Au core-Ag shell nanorods (Au-MBA@Ag NRs) were prepared by a seed-mediated growth method, then loaded on octahedral MIL-88B-NH_2 to obtain a novel ratiometric SERS substrate of Au-MBA@Ag NRs/PSS/MIL-88B-NH_2 (AMAPM) for detecting rhodamine 6G (R6G) in chili powder. The porous structure and excellent adsorption ability of MIL-88B-NH_2, allowed for increased loading of Au-MBA@Ag NRs, thereby shortening the distance between adsorbed R6G and the "hot spot" resulting from local surface plasmon resonance (LSPR) of Au-MBA@Ag NRs. Based on the SERS characteristic peak ratio of R6G to 4-MBA, the ratiometric SERS substrate displayed improved accuracy and excellent performance for R6G detection, with a wide linear range of 5–320 nM and a low detection limit of 2.29 nM as well as fine stability, reproducibility and specificity. The proposed ratiometric SERS substrate offered a simple, fast and sensitive sensing strategy for R6G detection in chili powder, which demonstrated potential applications in food safety and the analysis of trace analytes in complex matrices.

Received 6th February 2023
Accepted 24th March 2023

DOI: 10.1039/d3ra00790a

rsc.li/rsc-advances

1. Introduction

In recent years, the development of socioeconomics has made food safety an important issue for both industry and consumers, as it directly impacts people's health and even their lives.[1] During the production process of food, numerous contaminants, including pesticides, antibiotics, toxins, bacterial and heavy metals, may remain or be illegally added in food, posing a significant risk to consumers. Rhodamine 6G (R6G), a derivative of xanthene dye, has been widely used in agriculture, textile, paper and printing industries, but it is highly toxic to the human body and other organisms so it is strictly banned in the food industry.[2] However, due to the intense pink color and low cost, R6G is often illegally added in food to attract consumers. Therefore, a simple, fast and sensitive detection method for trace R6G in food with complex matrices is an urgent requirement for food safety.

Over the past decades, various detection techniques, such as fluorescence, HPLC, MS, and LC-MS,[3–6] have been used to detect R6G in food. However, these methods still suffer from tedious pre-treatment, expensive instruments, and time-consuming procedures which greatly limit the rapid and on-site detection. In contrast, surface-enhanced Raman spectroscopy (SERS) has gained enormous concern due to the excellent detection ability of simple, rapid, highly sensitive and non-invasive, so it has been applied to detect trace analytes in medicine, food and the environment.[7,8] However, traditional noble metal nanoparticles based SERS substrates are non-selective and susceptible to sample matrix.[9–11] Therefore, to enhance SERS performance and selectivity, some novel materials was used to construct functionalized SERS substrates, which have achieved more applications for high sensitive and selective detection of target substances.[12–14]

Metal–organic frameworks (MOFs) are one kind of crystalline porous materials with periodic network structures formed by self-assembly of organic ligands and metal ions or metal clusters through coordination reactions.[15] These materials have unique properties such as high specific surface area, good chemical stability and tunable structures,[16,17] which have received increased attention in many fields.[18–23] Benefited from the porous structure and large specific surface area, MOFs could load more noble metal nanoparticles and adsorb more target molecules on its surface and pores, which allowed the target molecule to be closer to "hot spot" generated by the local surface plasmon resonance (LSPR) of noble metal

[a]*Antibiotics Research and Re-Evaluation Key Laboratory of Sichuan Province, Chengdu University, Chengdu, 610106, China*

[b]*Key Laboratory of Medicinal and Edible Plants Resources Development of Sichuan Education Department, Sichuan Industrial Institute of Antibiotics, Chengdu University, Chengdu, 610106, China. E-mail: liaowenlong@cdu.edu.cn; liukunping@cdu.edu.cn; Fax: +86-28-8521-6578; Tel: +86-28-8521-6578*

[c]*School of Food and Biological Engineering, Chengdu University, Chengdu, 610106, China*

[d]*Institute for Advanced Study, Chengdu University, Chengdu, 610106, China*

† Electronic supplementary information (ESI) available. See DOI: https://doi.org/10.1039/d3ra00790a

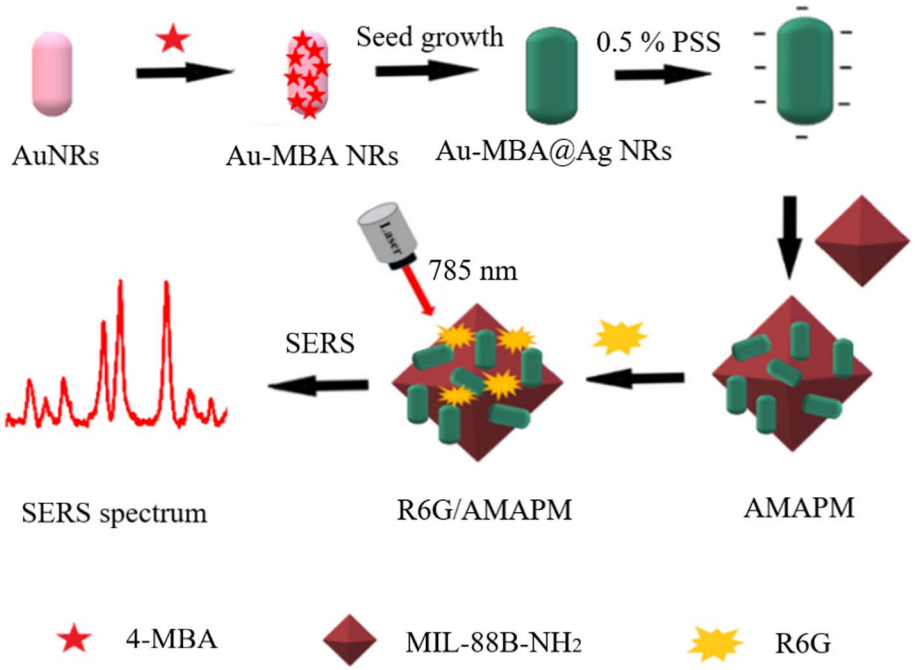

Scheme 1 Preparation of AMAPM substrates and SERS detection of R6G.

nanomaterials. Therefore, MOFs may be an ideal substrate for the construction of novel composite SERS substrate for sensitive detection of R6G.

In this study, we developed a simple and sensitive ratiometric SERS sensing strategy based on MOFs for the detection of R6G in chili powder (Scheme 1). Firstly, internal standard SERS nanoprobes based on Au@Ag core–shell nanorods (NRs) embedded with 4-mercaptobenzoic acid (4-MBA) (Au-MBA@Ag NRs) were prepared by a seed-mediated growth method. Next, octahedral MIL-88B-NH_2 was synthesized by a microwave-assisted method, then loading with poly (sodium 4-styrenesulfonate) (PSS) threated Au-MBA@Ag NRs through electrostatic interaction, thus a novel ratiometric SERS substrate of Au-MBA@Ag NRs/PSS/MIL-88B-NH_2 (AMAPM) was obtained. The porous structure and the fine adsorption ability of MOFs enhanced the loading of Au-MBA@Ag NRs as well as the adsorption of R6G, which could shorten the distance between R6G and LSPR resulted "hot spot" to enhance the SERS signals. Based on the SERS characteristic peak ratio of R6G to the internal standard molecule 4-MBA in AMAPM, the novel ratiometric SERS substrate displayed improved accuracy and excellent detection performance for R6G, with a wide linear range, low detection limit, and fine stability, reproducibility and specificity. Therefore, this work paved a new approach to food safety detection using MOFs based ratiometric SERS sensors.

2. Experiments

2.1 Chemicals and materials

2-aminoterephthalic acid (NH_2–H_2BDC, 98.0%) was purchased from Shanghai Titan Scientific Co., Ltd (Shanghai, China). Poly (sodium 4-styrenesulfonate) solution (PSS, 30 wt% in H_2O, Mw = 70 000), $HAuCl_4 \cdot 3H_2O$, L-ascorbic acid (AA) and 4-mercaptobenzoic acid (4-MBA) were purchased from Sigma-Aldrich (Shanghai, China). $FeCl_3 \cdot 6H_2O$, cetyltrimethylammonium bromide (CTAB), silver nitrate ($AgNO_3$) and *N*,*N*-dimethylformamide (DMF) were purchased from Chengdu Kelong Co., Ltd (Chengdu, China). Hexadecetyltrimethylammonium chloride (CTAC), rhodamine 6G (R6G) were purchased from Shanghai Aladdin Biochemical Technology Co., Ltd (Shanghai, China). All reagents were used without further purification, and experimental water was Milli Q water with a resistance of 18.2 MΩ cm. All glass apparatuses and stir bars were immersed in freshly prepared aqua regia solution ($V(HCl) : V(HNO_3) = 3 : 1$) overnight, and then washed several times with water.

2.2 Instruments

In this work, a homemade portable Raman device was used for SERS detection, which included a semiconductor CW laser operating at 785 nm (Laser 785-5HF, Oceanhood, Shanghai) with controllable power over the range of 0–500 mW, and a compact Raman spectrometer (NOVA, Ideaoptics, Shanghai) with a blazed grating of 600 line per mm, furthermore, a 3-axis stage (RB13M/M, Thorlabs, USA) was used to place the silicon chip for test, the laser power was set to 150 mW, and the spectral acquisition time was set to 5 s. Microwave device (MDS-6G, SINEO, Shanghai) was used to synthesis the MIL-88B-NH_2. Zeta potentiometer (NanoBrook 90Plus PALS, America), transmission electron microscopy (TEM, Talos F200S G2, Germany), scanning electron microscopy (SEM, Thermo scientific Apreo 2C, America), Fourier transform infrared spectrometer (FT-IR, Nicolet iS10, America), X-ray diffraction (XRD, Rigaku Ultima IV, Japan) and UV-visible spectrophotometer (UV-vis, Shimadzu UV-2600, Japan) were performed to characterize nanomaterials.

Fluorescence spectrophotometer (FL, Hitachi F-7000, Japan) was used to determine the adsorption efficiency of R6G.

2.3 Preparation of internal standard SERS nanoprobe (Au-MBA@Ag NRs)

Firstly, Au NRs were prepared by a classical seed-mediated growth method.[24,25] Briefly, 0.6 mL of newly prepared and frozen $NaBH_4$ (0.01 M) aqueous solution was added into the 10 mL mixed solution of CTAB (0.1 M) and $HAuCl_4$ (0.25 mM) with vigorous stirring, and reacted for 2 min to form a brown-yellow solution. Then, the prepared seed solution was kept in a water bath at 30 °C for 2 h. As for preparation of the growth solution, 50 mL CTAB (0.2 M), 330 μL $AgNO_3$ (0.04 M), 50 mL $HAuCl_4$ (0.25 mM) and 500 μL AA (0.1 M) were added to the solution successively under gentle stirring, and the color of solution changed from dark yellow to colorless. Then, 120 μL prepared seed solution was added to the mixture under mild stirring. The purplish red solution was obtained by water bath at 30 °C for 6 h, then the products were centrifuged at 12 000 rpm for 10 min, washed with water, and finally dispersed in 10 mL water. Secondly, 10 μL 4-MBA ethanol solution (0.1 mM) was added into 1 mL of Au NRs and incubated overnight to prepare Au-MBA NRs, after centrifuged at 12 000 rpm for 10 min, the products were dispersed into 3 mL CTAC (0.02 M), the internal standard molecule 4-MBA was loaded on the surface of Au NRs by strong Au–S bond.[26,27] Finally, the internal standard SERS nanoprobes were prepared by shell growth method,[28] 6 μL $AgNO_3$ (0.1 M) and 24 μL AA (0.1 M) were added in Au-MBA NRs solution and stirred for 1 min. Then the mixture was placed in a water bath maintained at 65 °C for 2.5 h, centrifuged and dispersed in 1 mL water.

2.4 Preparation of MIL-88B-NH_2

MIL-88B-NH_2 was prepared according to the reported literature with slight modification.[29] Briefly, 417 mg NH_2–H_2BDC and 622 mg $FeCl_3 \cdot 6H_2O$ were added to 50 mL DMF. The mixture was homogenized by ultrasound for 10 min, then transferred into a 4-polytetrafluoroethylene reactor and heated at 150 °C for 20 min using a microwave machine at the power of 300 W. Then, the reddish-brown crystals of MIL-88B-NH_2 were washed with DMF three times followed by $CHCl_3$ replacement. Finally, the as-prepared MIL-88B-NH_2 were stored at 4 °C after vacuum drying.

2.5 Preparation of MOFs based SERS substrate

5 mL as-prepared Au-MBA@Ag NRs were added in 5 mL PSS (0.5%, w/v in H_2O) followed by 20 min shaking. After centrifuging at 10 000 rpm, the PSS wraped Au-MBA@Ag NRs (Au-MBA@Ag NRs/PSS) were washed three times with water to remove residual PSS and dispersed in 5 mL water. Next, 1 mL Au-MBA@Ag NRs/PSS was added to 2 mL MIL-88B-NH_2 aqueous dispersion (1 mg mL^{-1}) following 20 min shaking. Then the obtained MOFs based SERS substrate of Au-MBA@Ag NRs/PSS/MIL-88B-NH_2 (AMAPM) was centrifuged and washed three times with water. Finally, the obtained AMAPM SERS substrate was dispersed in 2 mL water and stored at 4 °C.

2.6 SERS measurements

479 mg R6G was dissolved in 100 mL water (1 mM) as the stock solution for further use. The pH of R6G aqueous solution with different concentrations was adjusted to 5 with dilute hydrochloric acid, and the ionic strength was adjusted to 0.02 (mol L^{-1}) with NaCl (0.1 M). 125 μL Au-MBA@Ag NRs or 250 μL AMAPM was mixed with 1 mL R6G aqueous solution with different concentrations, and incubated at room temperature for 60 min. Next, the dispersion was centrifuged at 8000 rpm for 10 min to obtain the nano composite of R6G/Au-MBA@Ag NRs or R6G/AMAPM, which was then dispersed in 50 μL water for direct SERS detection. All data were obtained from three parallel experiments. The characteristic peak intensity ratio of R6G to the internal standard molecule 4-MBA was used for quantitative analysis.

2.7 Real sample detection

Chili powder produced by four manufacturers was purchased from the local market. Before SERS measurement, four chili powder samples were treated using the following method. Briefly, 1.00 g of chili powder was extracted with 20 mL of methanol : water (1 : 1, v/v) for 30 min and then the solid was then filtrated and washed three times with 20 mL of methanol : water (1 : 1, v/v). All supernatant was collected and diluted 20 times with water. After the pH and ionic strength were adjusted to 5 and 0.02 (mol L^{-1}), respectively, the obtained sample solution was applied for SERS detection using the above optimal SERS condition.

3. Results and discussion

3.1 Characterization of Au-MBA@Ag NRs

Au NRs were selected as the seeds for the fabrication of Au@Ag core–shell NRs due to their anisotropic shapes that can generate a strong electromagnetic field.[30] As can be seen from Fig. 1A, Au NRs had a rod structure of about 40 nm in length and 10 nm in width. The UV-vis spectrum of Au NRs (Fig. 1B) displayed two surface plasmon resonance (SPR) bands that referred to transverse and longitudinal plasmon bands. The strong band at 733 nm resulted from the resonant propagation of surface plasmon along the longitudinal axis, another weak band at 515 nm was attributed to the presence of impurities or a small amount of spherical gold nanoparticles in Au NRs solution.[30] After modification of 4-MBA on Au NRs, the SPR band was red-shifted from 733 nm to 756 nm, indicating that 4-MBA was successfully grafted onto Au NRs.

The SERS performance of Au-MBA@Ag NRs was affected by the thickness of silver shell. For Au@Ag core–shell nanostructure, nanoparticles with thin Ag shells on Au cores had similar optical properties to pure Ag NP.[31] In this work, the amount of $AgNO_3$ was optimized during the preparation of Au-MBA@Ag NRs (S1 in ESI†). As shown in Fig. 1C, the TEM image of Au-MBA@Ag NRs prepared by 6 μL $AgNO_3$ (0.1 M) and 24 μL AA (0.1 M) showed a rod-like structure about 50 nm in length and 20 nm in width with obvious core–shell structure, and the thickness of Ag shell was about 5 nm. UV-vis spectra and colors

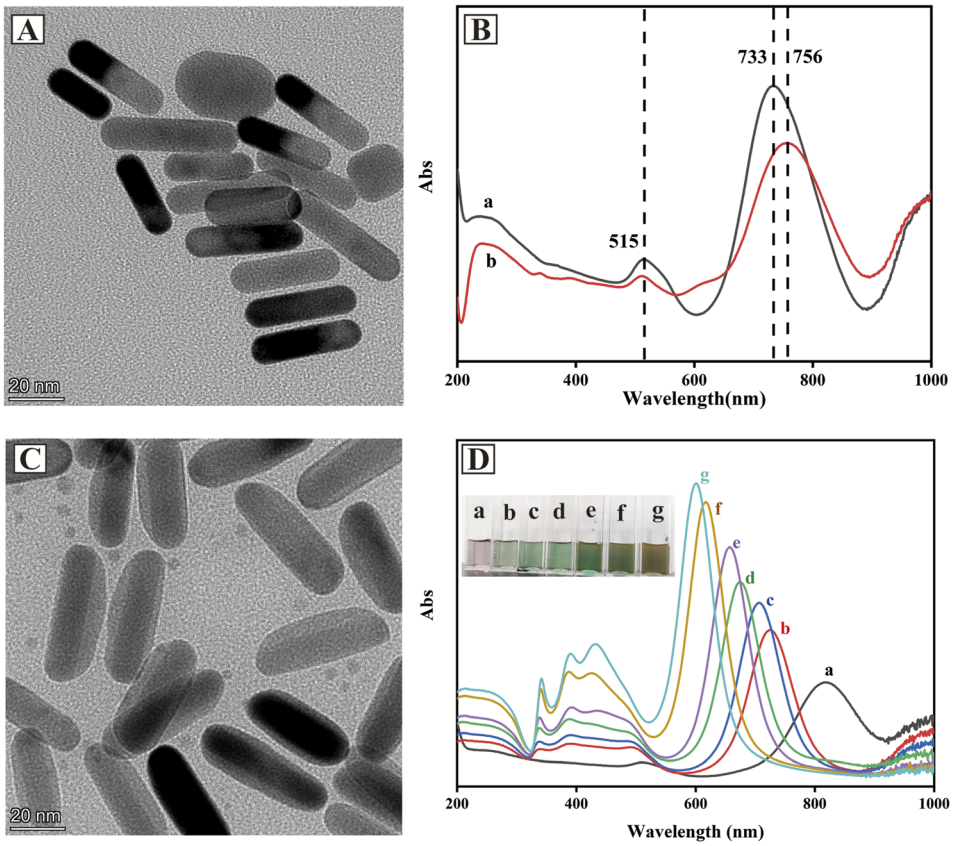

Fig. 1 (A) TEM image of Au NRs. (B) Uv-vis spectra of Au NRs (a) and Au-MBA NRs (b). (C) TEM image of Au-MBA@Ag NRs prepared at 6 μL $AgNO_3$ (0.1 M) and 24 μLAA (0.1 M). (D) Uv-vis spectra of Au-MBA@Ag NRs prepared with different amounts of $AgNO_3$ (0.1 M) and AA (0.1 M): (a) 0 μL and 0 μL, (b) 4 μL and 16 μL, (c) 6 μL and 24 μL, (d) 8 μL and 32 μL, (e) 10 μL and 40 μL, (f) 12 μL and 48 μL, (g) 14 μL and 56 μL. The inset image was the digital photo of corresponding Au-MBA@Ag NRs dispersion.

of Au-MBA@Ag NRs prepared with different amounts of $AgNO_3$ (0.1 M) and AA (0.1 M) are shown in Fig. 1D. With the increase of $AgNO_3$ and AA, the SPR bands of Au gradually blue-shifted and the intensity of characteristic peaks also increased. Meanwhile, the SPR bands of Ag (about 400 nm) gradually appeared and the intensity increased. The color of Au-MBA@Ag NRs gradually transferred from light purple to green and then brown.

To evaluate the SERS performances of Au-MBA@Ag NRs prepared with different amounts of $AgNO_3$, R6G was used as the probe molecule for the evaluation. As can be seen from Fig. 2A, the characteristic peaks of 4-MBA at 1077 cm^{-1} ($\nu_{(C-S)}$ aromatic stretching), 1585 cm^{-1} ($\nu_{(C-C)}$ stretching) and that of R6G at 612 cm^{-1} (C–C–C ring in-plane vibration movement), 773 cm^{-1} ($\delta_{oop\ (C-H)}$ stretching), 1313 cm^{-1} (xanthene core and amide group), 1363 cm^{-1} (xanthene core and amide group), 1511 cm^{-1} ($\upsilon_{s(C-C)}$ stretching) could be obviously observed in the SERS spectra by using Au@Ag NRs as SERS substrate.[32–34] Additionally, the SERS performance for R6G detection of Au-MBA@Ag

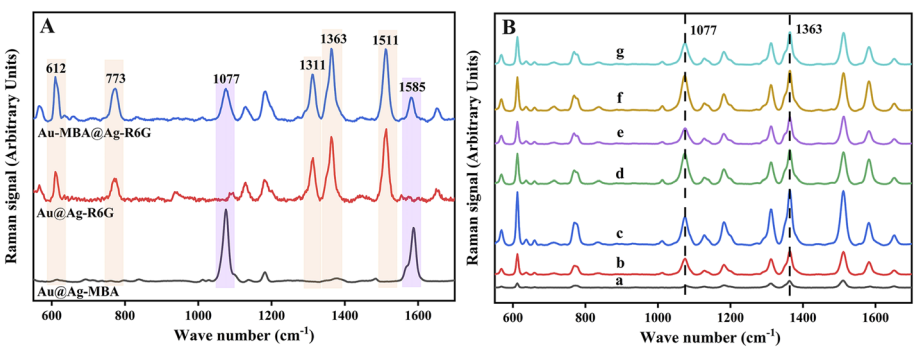

Fig. 2 (A) SERS spectra of Au@Ag-MBA, Au@Ag-R6G and Au-MBA@Ag-R6G. (B) SERS performances for R6G (10 μm) detection of Au-MBA@Ag NRs prepared with different amounts of $AgNO_3$ (0.1 M) and AA (0.1 M): (a) 0 μL and 0 μL, (b) 4 μL and 16 μL, (c) 6 μL and 24 μL, (d) 8 μL and 32 μL, (e) 10 μL and 40 μL, (f) 12 μL and 48 μL, (g) 14 μL and 56 μL.

NRs prepared with different amounts of $AgNO_3$ (0.1 M) and AA (0.1 M) were compared. As shown in Fig. 2B, the best SERS performance of Au-MBA@Ag NRs was achieved by adding 6 μL of $AgNO_3$ (0.1 M) and 24 μL of AA (0.1 M), so they were selected as the optimal preparation amount for Au-MBA@Ag NRs preparation.

Fig. S1† shows the Zeta potentials of Au NRs, Au-MBA NRs and Au-MBA@Ag NRs prepared with 6 μL $AgNO_3$ (0.1 M) and 24 μL AA (0.1 M). The positive charge of Au NRs was probably due to the adsorbed CTAB which was used as a protective agent during the preparation process. After 4-MBA grafted onto Au NRs *via* Au–S bond, the positive charge of Au-MBA NRs decreased. The binding of 4-MBA may have led to the desorption of CTAB from Au NRs surface. Then the positive charge of Au-MBA@Ag NRs was increased compared to Au-MBA NRs, which might due to the adsorption of CTAC during the preparation of Au-MBA@Ag NRs. The change of Zeta potential was obvious evidence for the successful preparation of Au-MBA@Ag NRs SERS nanoprobes.

3.2 Characterization of MIL-88B-NH_2

Fe-based MOFs of MIL-88B-NH_2 were prepared by a microwave-assisted method. As shown in Fig. 3A, the morphology of MIL-88B-NH_2 displayed a regular octahedral shape with a particle size of 200–300 nm. As can be seen from Fig. S2,† the XRD peaks at 6.6° (100), 8.8° (101), 9.0° (102), 16.3° (200), 16.8° (103), 17.8° (202), 20.0° (210), 22.0° (212), 24.8° (300) and 27.0° (311) suggested that MIL-88B-NH_2 obtained a highly crystalline structure and successfully fabricated by a microwave-assisted method.[35,36] Additionally, as shown in Fig. 3B, the FT-IR absorption peaks at 3338 cm^{-1} (N–H), 3470 cm^{-1} (N–H), 1655 cm^{-1} (C=O), 1579 cm^{-1} (C=C), 1385 cm^{-1} (C–O), 1258 cm^{-1} (C–N), 770 cm^{-1} (Fe–O–Fe) and 571 cm^{-1} (Fe–O–Fe) also clearly demonstrated the successful preparation of MIL-88B-NH_2.[29]

3.3 Characterization of MOFs based SERS substrate

To prepare AMAPM, the as-prepared Au-MBA@Ag NRs were first functionalized by PSS through a non-covalent method to obtain PSS wrapped Au-MBA@Ag NRs (Au-MBA@Ag NRs/PSS). Then, by electrostatic self-assembly process, the negative Au-MBA@Ag NRs/PSS was self-assembled on MIL-88B-NH_2 to obtain AMAPM. The preparation ratio (volume ratio, v/v) of MIL-88B-NH_2 to Au-MBA@Ag NRs/PSS was also optimized (S2 in ESI†). As shown in Fig. S3,† in which the adsorption percentage of R6G and the ratio of characteristic peak intensity of 1363 cm^{-1} (R6G) to 1077 cm^{-1} (4-MBA) were used to evaluate the adsorption efficiency and SERS performance of R6G, respectively. When the preparation ratio was 2 : 1, both adsorption efficiency and SERS performance for R6G were the best. As shown in Fig. 3C, after the decoration of Au-MBA@Ag NRs/PSS by electrostatic

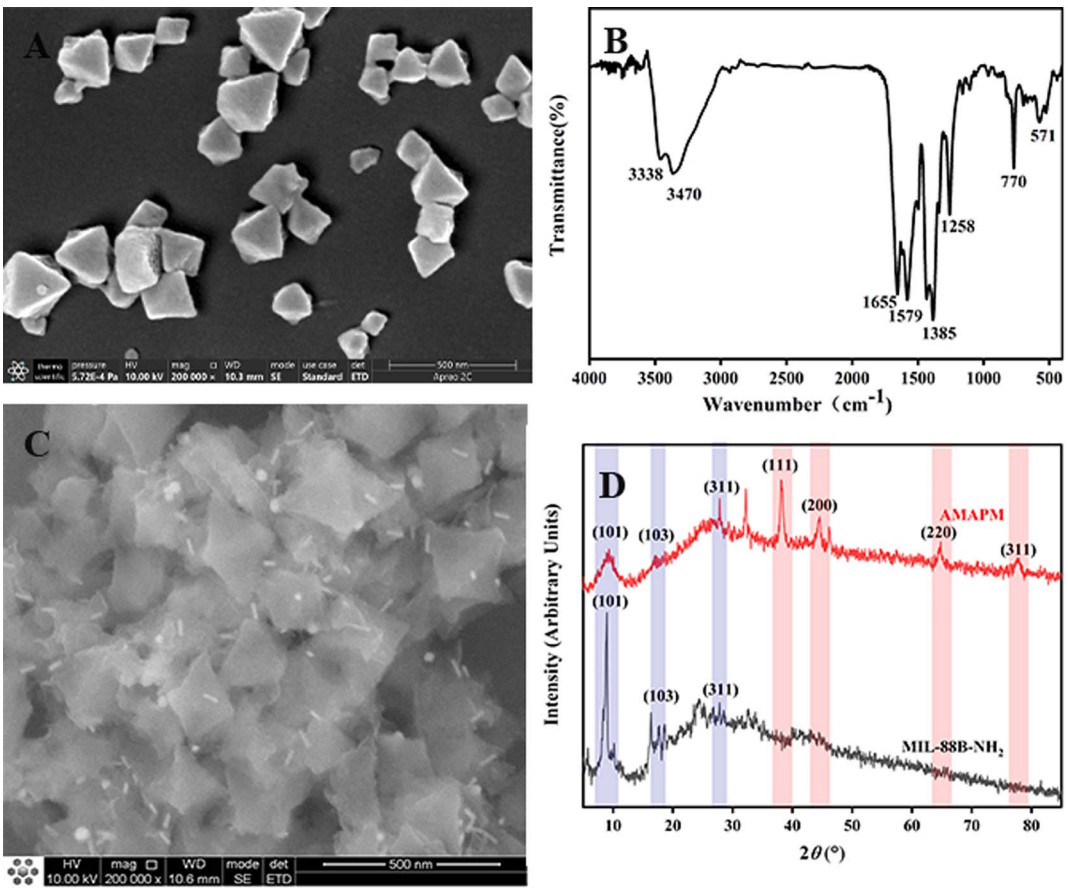

Fig. 3 (A) SEM image of MIL-88B-NH_2. (B) FT-IR spectrum of MIL-88B-NH_2. (C) SEM image of AMAPM. (D) XRD patterns of MIL-88B-NH_2 and AMAPM (5–85°).

adsorption on the surface of MIL-88B-NH_2 to obtain AMAPM, the rod-like Au-MBA@Ag NRs were evenly distributed on the surface of MIL-88B-NH_2 and the octahedral morphology of MIL-88B-NH_2 was still well maintained. Furthermore, from the comparision of XRD in Fig. 3D between MIL-88B-NH_2 and AMAPM, except the diffraction peaks of MIL-88B-NH_2 at 8.8° (101), 16.8° (103), 27.0° (311), AMAPM also displayed additional diffraction peaks of Au and Ag at 38.3° (111), 44.3° (200), 64.8° (220) and 78.1° (311), which demonstrated that the crystallinity of the loaded Au-MBA@Ag NRs was good and the crystal structure of MOFs was not damaged after AMAPM construction.

Meanwhile, Zeta potential was also used to confirm the assemble process of AMAPM. As shown in Fig. S4,† Au-MBA@Ag NRs and MIL-88B-NH_2 exhibited a positive potential of 13.54 mV and 22.94 mV, respectively. In order to assemble Au-MBA@Ag NRs on the surface of MIL-88B-NH_2, Au-MBA@Ag NRs were wrapped with PSS and the Zeta potential of Au-MBA@Ag NRs/PSS reversed to −32.80 mV. After decoration of Au-MBA@Ag NRs/PSS on the surface of MIL-88B-NH_2 through electrostatic interaction, the prepared AMAPM showed a weak positive potential of 1.83 mV which hinted the successful preparation of AMAPM. Due to the high adsorption effect originated from the large specific surface of MIL-88B-NH_2 and the excellent SERS performance of Au-MBA@Ag NRs on AMAPM, the AMAPM SERS substrate maybe exhibited good detection ability for R6G.

3.4 Optimization of SERS detection conditions

To obtain optimal adsorption effect and SERS performance for R6G, the SERS detection conditions based on AMAPM were optimized (S3–S6 in ESI†). As shown in Fig. S5,† with the increase in AMAPM amounts, the adsorption efficiency for R6G gradually increased. However, when the amounts of AMAPM exceeded 250 μL, the adsorption efficiency didn't increase significantly. From Fig. S6,† when R6G adsorption time of AMAPM was more than 60 min, the adsorption efficiency increased slightly. In addition, both adsorption efficiency and SERS performance for R6G detection were the best when pH was 5 (Fig. S7†). As shown in Fig. S8,† the adsorption efficiency of R6G increased with the increase of ionic strength of the solution, but the SERS performance for R6G was the best when the ionic strength was 0.02 mol L^{-1}. After comprehensive consideration, 250 μL AMAPM, adsorption time of 60 min, pH 5 and ionic strength of 0.02 mol L^{-1} were selected as the optimum detection conditions in this work.

3.5 R6G detection based on AMAPM

Under optimal conditions, 1 mL R6G aqueous solutions with different concentrations were mixed with 125 μL of Au-MBA@Ag NRs or 250 μL AMAPM as SERS substrate and then used for the SERS measurement. For Au-MBA@Ag NRs substrate as shown in Fig. 4A–C, the Raman intensity of R6G characteristic peak at 1363 cm^{-1} increased generally with the increase of R6G concentration (Fig. 4A). In the concentration range of 20 to 160 nM, both the Raman intensity of 1363 cm^{-1} (Fig. 4B) and the ratio of intensity (I_{1363}/I_{1077}) (Fig. 4C) showed a linear relationship with the concentration of R6G with a correlation coefficient (R^2) of 0.9812 and 0.9861, indicating a poor correlation. Meanwhile, the error bar also hinted the existence of a large measurement error. In contrast, when using

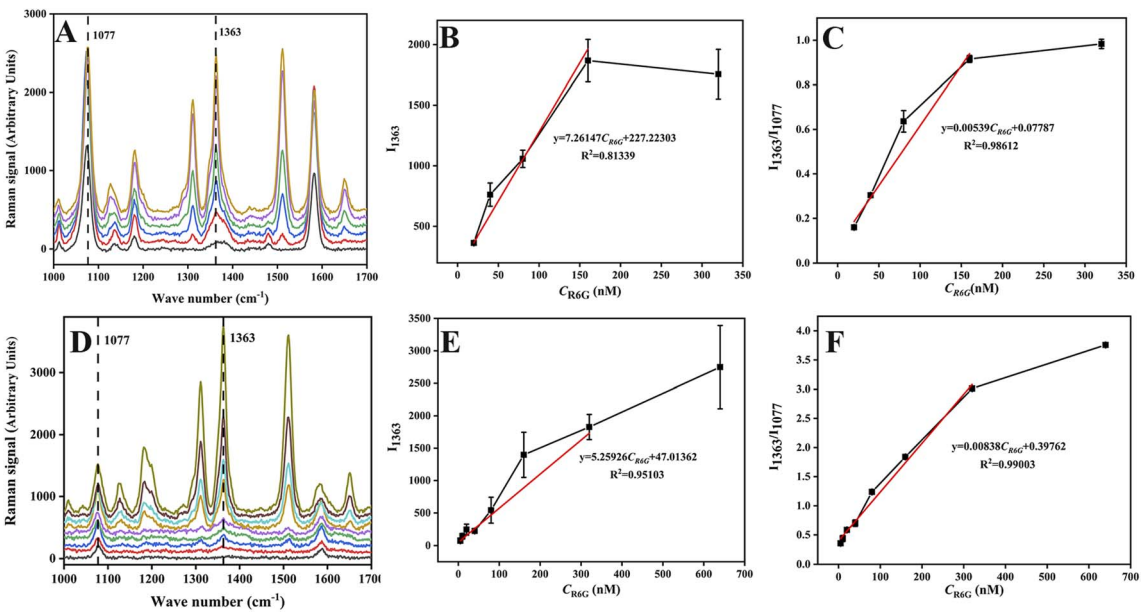

Fig. 4 (A) SERS spectra of R6G solution with different concentrations (0, 20, 40, 80, 160, 320 nM) using Au-MBA@Ag NRs as SERS substrate, (B) the linear relationship between SERS intensity at 1363 cm^{-1} and R6G concentration for Au-MBA@Ag NRs SERS substrate, (C) the linear relationship between the ratio of SERS signal intensity (I_{1363}/I_{1077}) and R6G concentration for Au-MBA@Ag NRs SERS substrate, (D) SERS spectra of R6G solution with different concentrations (0, 5, 10, 20, 40, 80, 160, 320, 640 nM) using AMAPM as SERS substrate, (E) the linear relationship between SERS intensity at 1363 cm^{-1} and R6G concentration for AMAPM SERS substrate and (F) the linear relationship between the ratio of SERS signal intensity (I_{1363}/I_{1077}) and R6G concentration for AMAPM SERS substrate.

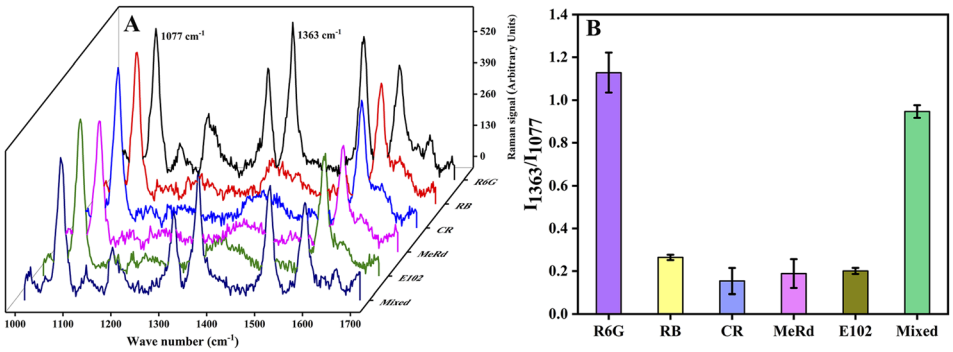

Fig. 5 (A) The SERS spectra and (B) SERS signal intensity at the AMAPM SERS substrate of R6G (80 nM), rhodamine B (RB, 1000 nM), methyl red (MeRd, 1000 nM), congo red (CR, 1000 nM), lemon yellow (E102, 1000 nM) and the mixed solution contained the same concentration of R6G and interferents at the same time.

the AMAPM substrate as shown in Fig. 4D–F, the Raman intensity of R6G characteristic peak at 1363 cm^{-1} increased generally with the increase of R6G concentration (Fig. 4D). The Raman intensity of 1363 cm^{-1} (Fig. 4E) showed a linear relationship with the concentration of R6G between 5 to 320 nM but got a poor R^2 of 0.9510 and a large error bar. However, for the ratio of intensity (I_{1363}/I_{1077}) (Fig. 4F), it exhibited improved accuracy and an excellent linear relationship with the concentration of R6G between 5 to 320 nM with good R^2 of 0.9900 and low limit of detection (LOD) of 2.29 nM (3σ). Thus, based on the fine adsorption effect of AMAPM substrate for R6G and the corrective action of the internal standard method using 4-MBA as the internal standard molecule, the ratiometric SERS sensor exhibited a wide linear range and fine sensitivity as well as high accuracy.

Additionally, this as-constructed SERS sensor had also been compared with numerous R6G detection methods reported in literature. As shown in Table S1,† traditional methods such as UV-vis, HPLC and fluorescence usually suffered from complex pretreatment, expensive instrument, and high detection limits. Although some SERS methods had also been developed, most SERS methods exhibited narrow linear ranges and high detection limits. However, for this as-constructed AMAPM based SERS sensor, both the detection limit and the linear range were improved and very good results were achieved. This could be attributed to the large specific surface area and the good adsorption effect for R6G of MOFs in AMAPM SERS substrate to keep the R6G molecule close to the Au-MBA@Ag NRs hot spot area to enhance the Raman signal.

3.6 Specificity, reproducibility and stability of the SERS sensor

Specificity, reproducibility and stability were important aspects for the performance evaluation of the SERS sensor. For specificity, a series of interferents including rhodamine B (RB, 1000 nM), methyl red (MeRd, 1000 nM), congo red (CR, 1000 nM), lemon yellow (E102, 1000 nM) were selected to evaluate specificity by measuring the SERS signals of these interferents under the same conditions and compared with R6G (80 nM). As shown in Fig. 5, with an excess (up tenfold) amount of interferents, there was almost no interference for R6G detection and the SERS sensor exhibited superior selectivity for R6G which contributed to the specific adsorption of AMAPM SERS substrate for R6G and then gave rise to the Raman signal for R6G. The results demonstrated that the AMAPM SERS sensor had good selectivity for R6G and the coexisting interferents had little or no influence on the detection of R6G. For reproducibility, the detection of R6G (80 nM) was repeated 6 times under the same detection condition. As shown in Fig. S9,† the relative standard deviation (RSD) of I_{1363} obtained in 6 detections was 22.21%. However, the RSD of I_{1363}/I_{1077} obtained in 6 detections was only 4.69%, which indicated that the ratiometric SERS method based on AMAPM SERS substrate could effectively overcome environmental interference and make the results more reproducible, thus ensuring the accuracy of the results. For stability, 10 copies of AMAPM SERS substrate were stored at 4 °C and 1 copy was taken out for the SERS signals detection under the optimal conditions every 2 days up to 20 days. As shown in Fig. S10,† according to the SERS signal intensity (1077 cm^{-1}) of 4-MBA on the AMAPM SERS substrate, the RSD was only 4.56%

Table 1 Recovery of detection R6G in chili powder sample

	Measured concentration (nM)					
Concentration of addition (nM)	1	2	3	Average	Recovery (%)	RSD (%)
20	19.68	17.02	19.11	18.60	93.02	7.53
40	43.16	39.50	41.10	41.25	103.13	4.44
80	80.96	80.79	80.46	80.74	100.92	0.32

within 20 days, indicating that the AMAPM SERS substrate had good stability and potential application for detection of analytes.

3.7 Real sample analysis

The content of R6G in the four chili powder samples was determined under optimal SERS conditions and no R6G was detected in the four samples. One sample was selected to evaluate the accuracy of the method by the blank spiked recovery method. The SERS spectra of the real sample and spiked samples of chili powder are shown in Fig. S11,† no R6G was detected in the blank chili powder samples, while obvious SERS signals of R6G were collected after being spiked with different concentrations. As shown in Table 1, the recoveries of R6G from three concentrations were 93.02–103.13%, and RSD were 0.32–7.53%, indicating that this ratiometric SERS sensor could achieve accurate and sensitive detection of R6G in chili powder samples.

4. Conclusions

In conclusion, a ratiometric SERS substrate was successfully prepared by decorating MIL-88B-NH_2 with Au-MBA@Ag NRs and applied for the detection of R6G in chili powder. The porous structure and fine adsorption ability of MIL-88B-NH_2, contributed to an elevated loading amount of Au-MBA@Ag NRs and adsorption amount of R6G on the AMAPM, resulting the enhanced SERS signals intensity. Based on the SERS characteristic peak ratio of R6G to the internal standard molecule 4-MBA in AMAPM, the constructed ratiometric SERS substrate displayed improved accuracy and excellent detection performance for R6G with a wide linear range and low detection limit, as well as fine stability, reproducibility and specificity. Real sample analysis confirmed the proposed ratiometric SERS sensing strategy as a simple, fast and sensitive method for detecting R6G in chili powder, which showed great application potential in food safety testing and the analysis of trace components in complex matrices.

Author contributions

Yangjie Chen: experimental research, formal analysis, methodology, writing-original draft. Juan Hao: experimental research, formal analysis, writing-original draft. Zhihang Yin: experimental research, formal analysis, writing-original draft. Qinghui Wang: experimental research. Youting Zhou: experimental research. Lingpu Jia: methodology, writing-review & editing. Huiming Li: methodology, writing-review & editing. Wenlong Liao: supervision, writing-review & editing. Kunping Liu: supervision, writing-review & editing, project administration.

Conflicts of interest

There are no conflicts to declare.

Acknowledgements

The authors acknowledge the support provided by Second Tibetan Plateau Scientific Expedition and Research Program (STEP) (No. 2019QZKK0201) and Sichuan Science and Technology Program (No. 2022YFQ0050).

Notes and references

1 B. X. Hu, H. B. Pu and D. W. Sun, Multifunctional cellulose based substrates for SERS smart sensing: Principles, applications and emerging trends for food safety detection, *Trends Food Sci. Technol.*, 2021, **110**, 304–320.
2 K. C. Behera, B. N. Patra and B. Bag, Dual mode detection of water in an organic solvent with a rhodamine-6G derivative, *Sens. Actuators, B*, 2021, **338**, 129861.
3 T. L. Chiang, Y. C. Wang and W. H. Ding, Trace determination of Rhodamine B and Rhodamine 6G Dyes in aqueous samples by solid-phase extraction and high-performance liquid chromatography coupled with fluorescence detection, *J. Chin. Chem. Soc.*, 2012, **59**(4), 515–519.
4 K. K. Chan, S. H. K. Yap, D. Giovanni, T. C. Sum and K. T. Yong, Water-stable perovskite quantum dots-based FRET nanosensor for the detection of Rhodamine 6G in water, food, and biological samples, *Microchem. J.*, 2022, **180**, 107624.
5 M. Arabi, A. Ostovan, A. R. Bagheri, X. Guo, J. Li, J. Ma and L. Chen, Hydrophilic molecularly imprinted nanospheres for the extraction of rhodamine B followed by HPLC analysis: A green approach and hazardous waste elimination, *Talanta*, 2020, **215**, 120933.
6 A. Tkaczyk-Wlizło, K. Mitrowska and T. Błądek, Quantification of twenty pharmacologically active dyes in water samples using UPLC-MS/MS, *Heliyon*, 2022, **8**(4), e09331.
7 H. K. Lee, Y. H. Lee, C. S. L. Koh, C. P. Q. Gia, X. M. Han, C. L. Lay, H. Y. F. Sim, Y. C. Kao, Q. An and X. Y. Ling, Designing surface-enhanced Raman scattering (SERS) platforms beyond hotspot engineering: emerging opportunities in analyte manipulations and hybrid materials, *Chem. Soc. Rev.*, 2019, **48**(3), 731–756.
8 T. Sakano, Y. Tanaka, R. Nishimura, *et al.*, Surface enhanced Raman scattering properties using Au-coated ZnO nanorods grown by two-step, off-axis pulsed laser deposition, *J. Phys. D: Appl. Phys.*, 2008, **41**(23), 235304.
9 C. H. Huang, A. L. Li, X. Y. Chen and T. Wang, Understanding the role of Metal-organic rrameworks in surface-enhanced raman scattering application, *Small*, 2020, **16**(43), 2004802.
10 D. Li, D. M. Yao, C. N. Li, Y. H. Luo, A. H. Liang, G. Q. Wen and Z. L. Jiang, Nanosol SERS quantitative analytical method: A review, *TrAC, Trends Anal. Chem.*, 2020, **127**, 115885.
11 S. E. J. Bell, G. Charron, E. Cortes, J. Kneipp, M. L. Chapelle, J. Langer, M. Prochazka, V. Tran and S. Schlucker, Towards reliable and quantitative surface-enhanced raman

scattering (SERS): from key parameters to good analytical practice, *Angew. Chem., Int. Ed.*, 2020, **59**(14), 5454–5462.

12 J. R. Xia, W. W. Li, M. T. Sun and H. T. Wang, Application of SERS in the detection of fungi, bacteria and viruses, *Nanomaterials*, 2020, **12**(20), 572.

13 S. T. R. Pang, T. X. Yang and L. L. He, Review of surface enhanced Raman spectroscopic (SERS) detection of synthetic chemical pesticides, *TrAC, Trends Anal. Chem.*, 2016, **85**, 73–82.

14 N. Li, J. S. Ye and Y. Ma, Stimuli-responsive SERS nanoprobes for multiplexing detection, *Sens. Actuators, B*, 2019, **281**, 977–982.

15 P. L. Wang, L. H. Xie, E. A. Joseph, J. R. Li, X. O. Su and H. C. Zhou, Metal-organic frameworks for food safety, *Chem. Rev.*, 2019, **119**(18), 10638–10690.

16 P. X. Wang, Y. Sun, X. Li, L. Wang, Y. Xu and G. Li, Recent advances in metal organic frameworks based surface enhanced raman scattering substrates: synthesis and applications, *Molecules*, 2021, **26**(1), 209.

17 T. H. Yu, C. H. Ho, C. Y. Wu, C. H. Chien, C. H. Lin and S. Lee, Metal-organic frameworks: a novel SERS substrate, *J. Raman Spectrosc.*, 2013, **44**(11), 1506–1511.

18 S. Dhaka, R. Kumar, A. Deep, M. B. Kurade, S. W. Ji and B. H. Jeon, Metal-organic frameworks (MOFs) for the removal of emerging contaminants from aquatic environments, *Coord. Chem. Rev.*, 2019, **380**, 330–352.

19 Z. Hasan and S. H. Jhung, Removal of hazardous organics from water using metal-organic frameworks (MOFs): Plausible mechanisms for selective adsorptions, *J. Hazard. Mater.*, 2015, **283**, 329–339.

20 D. N. Jiang, M. Chen, H. Wang, G. M. Zeng, D. L. Huang, M. Cheng, Y. Liu, W. J. Xue and Z. W. Wang, The application of different typological and structural MOFs-based materials for the dyes adsorption, *Coord. Chem. Rev.*, 2019, **380**, 471–483.

21 Y. Shi, A. F. Yang, C. S. Cao and B. Zhao, Applications of MOFs: Recent advances in photocatalytic hydrogen production from water, *Coord. Chem. Rev.*, 2019, **390**, 50–75.

22 S. Zhang, F. L. Rong, C. A. P. Guo, F. H. Duan, L. H. He, M. H. Wang, Z. H. Zhang, M. M. Kang and M. Du, Metal-organic frameworks (MOFs) based electrochemical biosensors for early cancer diagnosis in vitro, *Coord. Chem. Rev.*, 2021, **439**, 213948.

23 H. Daglar and S. Keskin, Recent advances, opportunities, and challenges in high-throughput computational screening of MOFs for gas separations, *Coord. Chem. Rev.*, 2020, **422**, 213470.

24 H. J. Chen, L. Shao, Q. Li and J. F. Wang, Gold nanorods and their plasmonic properties, *Chem. Soc. Rev.*, 2013, **42**(7), 2679–2724.

25 L. B. Wang, Y. Y. Zhu, L. G. Xu, W. Chen, H. Kuang, L. Q. Liu, A. Agarwal, C. L. Xu and N. A. Kotov, Side-by-side and end-to-end gold nanorod assemblies for environmental toxin sensing, *Angew. Chem., Int. Ed.*, 2010, **49**(32), 5472–5475.

26 W. L. Liao, Y. J. Chen, L. J. Huang, Y. Wang, Y. T. Zhou, Q. Tang, Z. M. Chen and K. P. Liu, A capillary-based SERS sensor for ultrasensitive and selective detection of Hg^{2+} by amalgamation with Au@4-MBA@Ag core-shell nanoparticles, *Microchim. Acta*, 2021, **188**(10), 354.

27 X. B. Huang, S. H. Wu, H. C. Hu and J. J. Sun, AuNanostar@4-MBA@Au core-shell nanostructure coupled with exonuclease III-assisted cycling amplification for ultrasensitive SERS detection of ochratoxin A, *ACS Sens.*, 2020, **5**(8), 2636–2643.

28 Y. Tian, G. H. Li, H. Zhang, L. L. Xu, A. X. Jiao, F. Chen and M. Chen, Construction of optimized Au@Ag core-shell nanorods for ultralow SERS detection of antibiotic levofloxacin molecules, *Opt. Express*, 2018, **26**(18), 23347–23358.

29 T. V. Tran, V. H. Nguyen, L. X. Nong, H. T. T. Nguyen, D. T. C. Nguyen, T. T. Nguyen, H. T. T. Nguyen and T. D. Nguyen, Hexagonal Fe-based MIL-88B nanocrystals with NH_2 functional groups accelerating oxytetracycline capture via hydrogen bonding, *Surf. Interfaces*, 2020, **20**, 100605.

30 F. K. Alsammarraie and M. S. Lin, Using standing gold nanorod arrays as surface-enhanced raman spectroscopy (SERS) substrates for detection of carbaryl residues in fruit juice and milk, *J. Agric. Food Chem.*, 2017, **65**(3), 666–674.

31 A. K. Samal, L. Polavarapu, S. Rodal-Cedeira, L. M. Liz-Marzan, J. Perez-Juste and I. Pastoriza-Santos, Size tunable Au@Ag core shell nanoparticles: synthesis and surface-enhanced raman scattering properties, *Langmuir*, 2013, **29**(48), 15076–15082.

32 F. W. Meng, X. Y. Ma, N. Duan, S. J. Wu, Y. Xia, Z. P. Wang and B. C. Xu, Ultrasensitive SERS aptasensor for the detection of oxytetracycline based on a gold-enhanced nano-assembly, *Talanta*, 2017, **165**, 412–418.

33 J. C. Wang, C. C. Qiu, X. J. Mu, H. Pang, X. C. Chen and D. M. Liu, Ultrasensitive SERS detection of rhodamine 6G and p-nitrophenol based on electrochemically roughened nano-Au film, *Talanta*, 2020, **210**, 120631.

34 Y. Sun, X. X. Yu, J. Y. Hu, X. M. Zhuang, J. J. Wang, H. X. Qiu, H. T. Ren, S. H. Zhang, Y. S. Zhang and Y. J. Hu, Constructing a highly sensitivity SERS sensor based on a magnetic metal-organic framework (MOF) to detect the trace of thiabendazole in fruit juice, *ACS Sustain. Chem. Eng.*, 2022, **10**(26), 8400–8410.

35 T. V. Tran, D. T. C. Nguyen, H. T. N. Le, D. V. N. Vo, V. D. Doan, V. P. Dinh, H. T. T. Nguyen, T. D. Nguyen and L. G. Bach, Amino-functionalized MIL-88B(Fe)-based porous carbon for enhanced adsorption toward ciprofloxacin pharmaceutical from aquatic solutions, *C. R. Chim.*, 2019, **22**(11–12), 804–812.

36 M. Y. Ma, A. Betard, I. Weber, N. S. Al-Hokbany, R. A. Fischer and N. Metzler-Nolte, Iron-based metal-organic frameworks MIL-88B and NH_2-MIL-88B: high quality microwave synthesis and solvent-induced lattice "breathing", *Cryst. Growth Des.*, 2013, **13**(6), 2286–2291.